Performance of a finned Activated Carbon Cloth - ethanol adsorption chiller

M. Tierney[1], L. Ketteringham, M. Azri Mohd Nor

1/ Corresponding author. Tel +44(0)117 3315903, e-mail mike.tierney@bristol.ac.uk

Department of Mechanical Engineering, University of Bristol, Queens Building, Bristol BS8 1TR, UK

Abstract

Measurements of cooling power and heat demand are presented for an adsorption heat pump (AHP) that integrated a finned adsorbent heat exchanger and a solar collector. For this study the adsorbent heat exchanger was heated/ cooled with fluid at near constant temperature. Results from a bench scale, large temperature jump (LTJ) test were scaled to predict the outcome of a larger experiment (adjusting for heat losses and additional heat capacities). The AHP's measured coefficients of performance were COP $\in$ [0.119, 0.236] versus COP $\in$ [0.233, 0.337] expected. The factor of discrepancy in specific cooling power (predicted cooling power divided by measured cooling power) is 1.1 to 2.0 versus a range of 2 to 6 suggested elsewhere. Although the scale-up procedure accounted for additional heat capacities, unwanted air ingress (even for mole fractions < 0.1%) might have substantially reduced adsorption/ evaporation rates.

Keywords: Adsorption heat pump, activated carbon cloth, finned-adsorbent, scale-up, LTJ

Highlights

- An AHP with finned adsorbent heat exchanger was constructed.
- A new method of scaling up calorimetric LTJ tests on small samples to predict SCP and COP is presented.
- Dynamic losses through vessel walls are important.
- The predicted SCP is 1.1 to 2.0 time measured value versus a ratio of 2 to 6 elsewhere.
- Air mole fractions < 0.1% might account for disparities in SCP and COP between prediction and measurement.

Nomenclature

A	area	m^2
b_{plug}	thickness of (brass) plug	m
c	specific heat capacity	J kg^{-1} K^{-1}
COP	coefficient of performance	
d_{HX}	outer diameter of heat exchanger	m
e_{RMS}	root mean square discrepancy between measured and predicted temperature	K
F	geometric factor	
h	specific enthalpy	J kg^{-1}
m	mass	kg
Q	heat transfer	J
r	radial co-ordinate	m
SCP	Specific cooling power	W kg^{-1}
T	temperature	K
U	overall heat transfer coefficient	W m^{-2} K^{-1}
X	adsorption loading	
X^*	Adsorption capacity	
V	volume	m^3
y	mole fraction	
z	vertical distance below start of condensate film	m

Greek symbols

α	heat transfer coefficient	W m^{-2} K^{-1}
λ	Thermal conductivity	W m^{-1} K^{-1}
ρ	density	kg m^{-3}
σ	Stefan-Boltzmann constant	W m^{-2} K^{-4}
τ	time constant	s
τ_{adiab}	time constant for evaporator load (corrected)	s
$\tau_{1/2}$	half cycle duration	s

Subscripts

a	all heat passing through fin base
a	refers to specific enthalpy of adsorbate
coil	heat transfer through evaporator or condenser
conv	convective component of heat transfer
fg	refers to heat of vaporisation
f	refers to saturated liquid
g	refers to saturated vapour
in	Refers to heat input
rad	radiative component of heat transfer
s	refers to saturation pressure
v	refers to superheated vapour
x	adsorbent

Superscripts

1,2	serial number used to indicated different estimate attempts
(a-l)	allows for heat losses
(a-lx)	allows for heat losses and sensible heat changes

1. Introduction

This paper concerns assessments of the thermal performance of a prototype adsorption heat pump (AHP) through direct measurement and through scale-up of small bench scale tests employing the "large temperature jump" (LTJ) [1]. Our objectives were as follows. (1) Originally funding was granted to build a chiller driven by concentrated sunlight. Owing to constraints associated largely with laboratory space and generator orientation the work does not cover a chiller designed for such operation, but a steam heated unit. (2) The operation of the chiller was to be predicted by scaling up data from bench-scale measurements, in order to accelerate machine development in future. The use of (constant) steam heating, rather than (variable) solar heating made the scale up procedure more reliable (prior to future work dealing with a variable underlying radiation intensity further complicated by the unrepeatable nature of cloud cover on sunlight).

A few companies have marketed AHPs or have near market machines (e.g. MyCon in Japan / Singapore, Valliant and Viessmann, both based in Germany). These units exploit sources of waste heat at temperatures as low as 50^{o}C, with coefficient of performance of roughly 0.4 and cooling power as low as 3 kW. These are used mostly for air conditioning where relatively high evaporator temperatures > 10^{o}C are acceptable. Per unit mass of adsorbent, cooling power is restricted by the low thermal conductivity of adsorbents. To improve metal-to-sorbent heat transfer, and shorten conduction paths lengths, one can adhere, press or coat adsorbent to fins [2][3]. Informative research reviews are available in [4] [5], [6].

LTJ offers a simpler, more representative approach than a mechanistic model of the adsorption heat exchanger. Such models deal with complex, coupled physical processes and require a large dataset [7] including intra-particle heat and mass transfer, particle-to-particle thermal resistance, particle-to-heat-exchanger thermal resistance and bed permeability. LTJ simply replicates the boundary conditions of the AHP, imposing these on a representative sample of adsorbent and then measuring the rate of refrigerant uptake (= adsorbate intake). In such a test, the sample is held at near constant pressure and the set point temperature undergoes a step change. The uptake is

65 determined from a small (~ 2 mbar) pressure change in a reservoir of adsorbate or (more recently)
66 by direct weighing.

67 Early measurements concerned "constant volume variable pressure" or V-LTJ [1]. The size of
68 the vapour holding tank constrained the vapour uptake and therefore constrained sample sizes.
69 Nonetheless Aristov et al [8] reports sample sizes as big as 314 mg with mono- or multiple layers of
70 Fuji silica RD grains. Aristov el al [8] suggested that the SCP for real adsorption coolers was 2-to-6
71 time lower than would have been expected from LTJ. This was attributed to (1) the temperature of
72 metal supports changed very quickly during LTJ but not so in real AHPs (2) the tests in [8] allowed
73 for large mass transfer surfaces and thin adsorbent layers. More recently realistic sections of AdHex
74 have been weighted directly, hence "G-LTJ" [9, 10]. Samples of up to 600 g were tackled with
75 claimed accuracy of 0.1 g. A complementary calorimetric approach [11] tackled samples in the range
76 of ~ 60g and the data from this approach is used here in the analysis of an AHP.

77 Our work was motivated by the construction of a solar chiller, designed so that the adsorption
78 heat exchanger could be illuminated directly by concentrated irradiation. As a first step in
79 understanding the adsorption heat exchanger, we have worked with "normal" boundary conditions -
80 both heating and cooling fluid were supplied at a nearly constant temperature. The selected pair was
81 activated carbon cloth (ACC)-ethanol. The paper presents the construction of the AHP and
82 summarises features of an earlier LTJ test on comparatively small samples of finned-surface-plus-
83 adsorbent. Heat balances indicated the importance of dynamic heat losses and steady heat losses
84 through the generator containment. In addition to the direct thermal measurements procedures to scale
85 up cooling power from the smaller LTJ tests are presented. Trend analysis and likely errors are
86 discussed in conjunction with results; a separate section discusses machine performance and future
87 improvements.

88

89

2 Methods and Material Properties

The section describes the construction of the chiller (Fig. 1), operating procedures, and material properties. Each experiment was broadly in two half-cycles. Firstly, steam heating of the generator, caused refrigerant to desorb, forcing it into the condenser coil (part 11). Secondly, water cooling of the generator caused refrigerant vapour to adsorb, forcing boiling in the evaporator coil (part 14). The essential features of smaller-scale measurements (under LTJ) are presented [11].

2.1 Construction of chiller

In essence the chiller comprised the generator, the evaporator, the condenser, and instrumentation.

To form the generator, the fin assembly was housed in glass tube, outer diameter 121-mm, with domed end (Fig. 1, item 2). Turnbull and Scott (Engineers) Ltd, Hawick, Scotland pressed square fins (item 17) hydraulically onto a copper tube-in-tube heat exchanger, with eleven ACC layers filling each fin-to-fin gap (items 1, 3, 4, 15, 16, 17). To render one side of the generator receptive to solar radiation the last 5mm of fin was bent to form a lip and coated with solar selective material. (The formation of 100 such lips was time consuming, requiring 150 person hours.) A brass plug sealed the open end of the glass tube and accommodated the heat exchanger (Fig. 1 items 1, 2, 4 and 4a). The glass tube was fabricated by glass blowers and the plug ground to fit snuggly therein (items 2, 4a). Under near vacuum, the assembly was leak tight to within 1 mbar of air ingress per day. However, the brass plug (mass 3.19 kg) promoted unwanted dynamic losses. The plug requires redesign in future – for example machineable ceramics [12] would reduce mass and thermal conductivity. (Their thermal conductivity is several hundred times lower than that of brass.)

The evaporator coil (item 14) was formed from a 2-m long, 22 mm-bore copper tube coiled six times, and similarly the condenser coil was formed from a 5-m length (item 11). A tank filled with 8-litres of water acted as the evaporator load (item 13), whereas a tank filled with 64-litres acted as the heat sink for the condenser (item 10). However, large temperature differences (up to 8 K, and reported in the next section) were evident between the evaporator load and (boiling) refrigerant and

likewise condensing refrigerant and the condenser's heat sink. Failure of condensate to drain freely into the sight tube (item 12), prevented reliable material balances.

Pressure gauges monitored the condenser, evaporator and generator (items 9) (Swagelok S series, pieozoresistive with calibration in the range 0 to 1 bar with claimed accuracy of 2.5 millibar within the best fit straight line.)

Temperature measurements supported a heat balance and computation of coefficient of performance and specific cooling power. Thermocouples (K-type) were fitted as follows: three within the ACC, on the mid-plane between fins; one sandwiched between the ACC and the fin lip; two monitoring fluid entering and leaving the tube-in-tube heat exchanger, three on the glass cover, one on the brass plug, three within the condenser heat sink, and three within the evaporator load. In addition, thermocouples were located on sections of pipework. To locate thermocouples within the generator a breakthrough was made, comprising a copper tube packed with epoxy resin. The claimed thermocouple accuracy was 0.5 K (mostly systematic error) but the observed repeatability was 0.03 K, owing to the electrical filters inside data loggers (Picologger TC-08).

2.2 Procedure

The experimental procedure follows. (1) All equipment was subjected to vacuum pump for 40 minutes and left overnight (the generator was open to the evaporator). (2) The following morning, the evacuation was repeated for 20 minutes. The generator was isolated and vacuumed further for 10 minutes. (3) The evaporator cooling load (item 13, Fig 1) and condenser heat sink (item 10) were filled with water at the required temperature of operation. (Weak brine was employed for temperatures close to freezing point.) The evaporator (item 14) was charged with 150 ml of ethanol. (4) The generator was isolated and heating applied (items 15, 16). The generator was connected to the condenser coil when their pressures matched. Heating was continued for the remainder of the half cycle. (5) The generator was isolated and water cooled. (6) The generator was opened to the evaporator coil when their pressures matched and cooling was continued for the remaining half cycle. Tests were repeated three times, in an attempt to reach a cyclic steady state.

Steam heating of the adsorption heat exchanger ensured a saturation temperature close to 100°C. The emerging condensate was captured in a vacuum flask mounted on a scale; as a cross-check, condensate volume was measured at the end of the experiment. Any sub-cooling of the condensate was to < 0.5 K.

All other heat flows were deduced from changes in the sensible energy of inventories of water. Heat dissipation from circulating pumps and stirrers was allowed for. When the generator was cooled process water was recirculated from a tank of 22 litres volume (the net heat input from the circulating pump was about 6% of cooling effect). To prevent its thermal stratification, the condenser heat sink (item 10) was stirred with a paddle, driven with a 4.3 watt motor and operated for 10% of the cooling time. The evaporator load (item 13) was stirred manually.

2.3 Material properties

The selected adsorbent was an activated carbon cloth, FM10 provided by Chemviron UK. The claimed BET surface area was 1400 $m^2\ g^{-1}$ and the nominal fibre diameter was 0.5-mm. Cloth was favoured because it could readily be cut to shape. The adsorbent was ethanol. (Methanol would be preferable owing to higher adsorption capacity and higher heat of vaporisation, however its toxicity was a concern (particularly as the chiller was periodically evacuated)).

Measurements on samples of a finned adsorbent are reported in [11]. Fig. 2 shows the fins and instrumentation. The heat release from the finned-adsorbent to the thermo-electric module (TEM , item 2) was deduced, and at the end of each experiment the mass gain by the adsorbent was recorded. The TEM controlled the temperature of the base of the sample and the cooling effect was inferred from module voltage, current and face temperature [13].

To impose LTJ the sample was exposed to vapour (typically at 20 mbar), held at constant temperature for ~ 2 hours, and a step change in the temperature of the sample base was applied. The temperature swing triggered (exothermic) adsorption. Notwithstanding complex, interrelated heat and mass transfer, rates of heat release versus time were fitted well to simple exponential functions. The

adsorption capacity of a sample was inferred at constant temperature but with a "large pressure jump" [14]. The measured heat transfer to the TEM was checked against gravimetric assessment.

Under LTJ, the rejection of heat through the fin base, $Q_a(t)$, was corrected to allow either for heat loss, or for heat loss plus changes in the sensible energy of the sample components.

$$Q^{(a-l)}(t) = Q_a(t) - Q_l(t) \quad [1]$$

$$Q^{(a-lx)}(t) = Q_a(t) - Q_l(t) - \sum Q_{x,i}(t) \quad [2]$$

where subscript a refers to raw measurement of heat rejection, subscript l refers to heat loss, and subscripts x,i refer to the changes in sensible energy (aluminium, activated carbon, adsorbate (ethanol)). These two estimates of heat rejection were both fitted well by exponential functions.

Correction of raw data for heat loss only (a-l)

$$Q^{(a-l)} = Q_o^{(a-l)}(1 - \exp(-t / \tau_{a-l})) \quad [3]$$

Full correction (a-lx)

$$Q^{(a-lx)} = Q_o^{(a-lx)}(1 - \exp(-t / \tau_{a-lx})) \quad [4]$$

Term $Q^{(a-l)}(t)$ characterised the heat transferred to the generator heating/ cooling fluid whereas $Q^{(a-lx)}(t)$ characterised the refrigerant mass adsorbed and hence the heat load on the evaporator. Time constants τ_{a-l} and τ_{a-lx} are reported in Table 1. Fig. 3 shows (a) representative heat release during adsorption under LTJ (b) the dependence of the adsorption capacity (X) on adsorption potential, inferred both calorimetrically and gravimetrically under LPJ.

Table 1 Time constants measured under LJT. ***Reprinted from Applied Thermal Engineering, vol. 93, M. Tierney et al. , Calorimetric Assessment of the Dynamics of a Finned Adsorbent. Copyright 2016, with permission from Elsevier.***

Base temp. T_b, K	Pressure, mbar	Correction for stray losses and sensible heat (a-lx)				Correction for stray losses only (a-l)		
		$Q_o^{a\text{-}lx}$, J	$m_x h_{ads} \Delta X^*$	$\tau_{a\text{-}lx}$, s	r^2	$Q_o^{a\text{-}l}$	$\tau_{a\text{-}l}$, s	r^2
338→303	22 to 27	-2264	-2167	183	0.9974	-3351	146	0.9910
338→303	13 to 16	-2403	-2480	185	0.9994	-3499	150	0.9940
360→303	20 to 24	-3554	-3654	191	0.9961	-5337	154	0.9983
358→323	21 to 23	-2308	-2000	159	0.9860	-3439	127	0.9695

The adsorption capacity X^* was fitted to the Dubinin-Radushkevich (DR) equation,

$$\ln(X^*) = -7\times10^{-7}\,(T\ln(p/p_s(T))^2 - 0.9206 \qquad [5]$$

where $p_s(T)$ is the saturation pressure. The maximum loading $X^*_m = 0.398$ was inferior to that of Unitika activated carbon fibres (ACF) measured by Sharkawy et al [15]: $X^*_m = 0.570$ for ACF-15 and $X^*_m = 0.797$ for ACF-20. Sharkawy et al found that heterogeneity constant n = 2 gave the best fit of the Dubinin Astakhov equation to data (i.e., Dubinin-Radushkevich applied). Promising recent developments wherein phenol resins were treated with two different mass ratios of KOH yielded X^*_m = 1.43 and 2.0 [16]. Brancato et al [17] report extensive measurements of properties and isortherms for commercial carbons and new synthesised porous composites (LiBr in a silica gel host matrix)

For purposes of the scale up, the heat rejection term $Q_o^{(a\text{-}lx)}$ (measured heat - losses – sensible heat) was not the directly measured value but related to the heat of adsorption and the isotherm , thus

$$Q_{o,pred}^{(a-lx)} = m_x\,(X^*_{end} - X^*_{start})\,\Delta h_{ads}\big|_{avg} \approx m_x \int_{Xstart^*}^{Xend^*} h_{fg}\,\frac{T}{T_s}\,dX^* \qquad [6]$$

where T_s is the saturation temperature, and $\Delta h_{ads} \approx h_{fg}\,T/T_s$ is the isosteric heat of adsorption (vapour to adsorbed phase) estimated according to Critoph [18] for DR equations. The root mean square discrepancy between measured and estimated values was 13.5% (LTJ and LPJ

tests were used in the same analysis - see Figure 4 and reference [11]). It is worth pointing out that whereas Critoph used Trouton's rule and the Clausius Clapeyron relationship more sophisticated estimates have since been postulated, e.g. Chakrobory et al [19] employ classical thermodynamics, Gibbs and Maxwell laws to estimate properties of adsorbed phase, including heat capacity, enthalpy, entropy, and isosteric heat of adsorption. The accuracy and theoretical basis of commonly used isotherms such as Toth and DA are still a matter for discussion, and note the recently modified isotherm in [20] (and have adapted their thinking to the adsorption of non polar gases and onto activated carbon in particular[21]).

The heat balance reported in the next section depends on the material properties and heat transfer coefficients summarised in Table 2.

Table 2 Material properties and correlations employed in heat balance and scale-up procedure (symbols used in the table are m, mass; c_p, specific heat; λ, thermal conductivity; ρ_{bulk}, bulk density; Nu, Nusselt number; Ra, Rayleigh number; Pr, Prandtl number)

Item	Material	Location (Fig. 1)	Properties
Miscellaneous parts			
Cover	Glass	2	m = 2.92 kg c_p = 750 J kg^{-1} K^{-1}
Plug	Brass	4A	m = 3.19 kg c_p = 377 J kg^{-1} K^{-1} λ = 109 W m^{-1} K^{-1} ρ = 8400 kg m^{-3}
Insulation	polyurethane foam	15, 16, pipework	λ = 0.03 W m^{-1} K^{-1} t = 1.0 cm
Parts of adsorption heat exchanger			
Adsorbent	Activated carbon cloth (ACC)	3	m = 0.63 kg c_p = 800 J kg^{-1} K^{-1} ρ_{bulk} = 258 kg m^{-3}
Adsorbed phase	Ethanol	-	m = 0.16 kg c_p = 377 J kg^{-1} K^{-1}
Heat exchanger tube	Copper	4	m = 0.73 kg c_p = 389 J kg-1 K-1
Fins	Aluminium	17	m = 0.75 kg c_p = 900 J kg^{-1} K^{-1} ρ = 2700 kg m^{-3} λ = 190 W m^{-1} K^{-1}
Heat Transfer Coefficients			
Cooling applied to brass plug, Dittus Boelter Equation [22]		4,4a	$Nu = 0.023\,\mathrm{Re}^{0.8}\,\mathrm{Pr}^{0.3}$
Heating applied to brass plug, Nusselt film theory [22] for local heat transfer coefficient.		4, 4a	$\alpha = \left[\frac{h_{fg}\,\rho_f\left(\rho_f-\rho_g\right)g\,\lambda_f^3}{4\,\mu\left(T_s-T_w\right)z}\right]^{1/4}$
Natural convection loss from surface of finned heat exchanger/ glass cover [23]		2, 3	$\bar{Nu}^{1/2} = 0.825 + \frac{0.387\,Ra^{1/6}}{\left[1+\left(0.492/\mathrm{Pr}\right)^{9/16}\right]^{8/27}}$

3. Energy balance and predictive modelling

An energy balance is drawn up for the experiment. Terms in the energy balance are adapted and used to scale up the results from tests on small samples (under LTJ).

With regard to directly measured heat addition/ rejection, Fig. 5 includes an outer control surface (item 1). Arrows indicate applied heat inputs (or outputs) and heat losses from pipework.

$$Q_{in}^{net} = \underbrace{\sum_i m_i\, c_i\, (T_i^{end} - T_i^{start})}_{sensible\ \ energy} + \underbrace{\int_{start}^{end} \sum_j U_j\, A_j\, (\bar{T}_j - T_{amb})\, dt}_{direct\ \ loss} + \ldots$$

$$\underbrace{m_x\, (X^{end} - X^{start})\, (h_a - h_f)}_{phase\ change} + \underbrace{m_k\, c_w \left(T_k^{end} - T_k^{start}\right)}_{coil\ loss} \qquad [7]$$

where Q_{in}^{net} is the net heat input to the generator and from Fig. 5 i ∈ {2, 3, 4, 5, 8, 11}, j ∈ {2, 3, 5, 8, 11} , k = 6 or 9. Subscript x refers to the mass of the ACC. Specific enthalpies h_a and h_f refer respectively adsorbed phase and the liquid phase. The phase change term was comparatively small, about 0.4% of Q_{in}^{net} so that $h_a - h_f$ could be approximated according to Hess's law

$$h_a(T_{gen}^{start}) - h_f\left(T_{cond}^{end}\right) \approx -\Delta h_{ads}\left(T_{gen}^{start}, X_{gen}^{start}\right) + \ldots$$
$$h_{fg}\left(T_{gen}^{start}\right) + c_{pl}\,(T_{cond} - T_{gen}^{start}) \qquad [8]$$

The end temperature of the evaporator load (k=9) was corrected for heat gain. On a typical plot of load temperature versus time (Fig. 6) point A represents the start of evaporation and the discontinuity at point B the end. The temperature rise from B to C was attributed to heat ingress and fitted to exponential recovery with its asymptote at ambient temperature and with characteristic time $\tau_{BC.}$ From A to D the hypothetical temperature achieved with a perfectly adiabatic load was

$$T_{adiab}(t) = T_{ABC}(t) - \int_{t_A}^{t} \frac{T_{amb}(t') - T_{ABC}(t')}{\tau_{BC}}\, dt' \qquad [9]$$

Fitting an exponential curve to AD yielded a characteristic time for evaporation, τ_{adiab}.

To scale up LTJ tests a control surface was drawn around the adsorption heat exchanger (item 4 on Fig. 5). The first attempt at scale up replaced the sensible heat correction allowing for the components of the heat exchanger and followed.

$$Q_{in}^{net,1} = \sum_i m_i\, c_i\, (\bar{T_i^{end}} - T_i^{start}) + \; Q_{o,pred}^{(a-lx)} \left(1 - \exp\left(-\frac{\tau_{1/2}}{\tau_{(a-lx)}} \right) \right) \qquad [10]$$

sensible energy *from LTJ*

where $\tau_{1/2}$ is the duration of the half-cycle, all heat capacities c_i of heat exchanger components (only) are reported in Table 2. Term $Q_{o,pred}^{(a\text{-}lx)}$ was found from Equation 6, with root mean square discrepancy of 13.5% between this prediction and measured values. Note that the mass ratio of fin to ACC was identical to that in bench-scale tests [11] but it was necessary to replace the heat capacity of an aluminium base (at bench-scale) with that of a copper tube (full scale).

A second estimate allowed for heat losses from the finned exchanger.

$$Q_{in}^{net,2} = Q_{in}^{net,1} + \sum_j m_j\, c_j\, (\bar{T_j^{end}} - T_j^{start}) \; + Q_{conv} + Q_{rad} + Q_{cond,plug} \qquad [11]$$

where Q_{conv} is convective loss from the adsorption heat exchanger (parts 3, 17 on Figure 1), Q_{rad} is the corresponding radiative loss and $Q_{cond,plug}$ is the loss from the heat exchanger inlet/ outlet to the brass plug (parts 4, 4a on Figure 1). The additional sensible heats are for the brass plug and glass cover. The heat loss components were found according to

$$Q_{conv} = \frac{A_{AdHex}}{\left(\frac{1}{\alpha_{AdHex}} + \frac{A_{AdHex}}{A_{cover}\, \alpha_{cover}} \right)} \int_{start}^{end} (T_{fin}^{tip}(t) - T_{cover}(t))\, dt \qquad [12]$$

$$Q_{rad} = \frac{A_{AdHex}\,\sigma}{\frac{1}{\varepsilon_{tip}} + \frac{1-\varepsilon_{glass}}{\varepsilon_{glass}}\left(\frac{A_{AdHex}}{A_{\text{cover}}}\right)} \int_{start}^{end} \left(T_{fin,tip}^4 - T_{\text{cover}}^4\right) dt \qquad [13]$$

$$Q_{cond,plug} = -\pi\, d_{HX}\, b_{plug} \lambda_{brass} \int_{start}^{end} \left.\frac{dT_{plug}}{dr}\right|_{(r=d_{HX}/2,t)} dt \qquad [14]$$

where b_{plug} is the plug thickness, d_{HX} is the diameter of the annular heat exchanger passing through the plug and λ is thermal conductivity. The heat transfer coefficients, α_{AdHex} and α_{cover}, were established from [23] for both laminar and turbulent natural convection from vertical surfaces (see also Table 2). The fin was idealised as annular such that the flank areas of idealised and real fins were equal. The surface areas A applied to the adsorption heat exchanger (or adhex) and the glass cover. The total hemispherical emissivity for glass was taken as 0.92 and that for the exchanger's exterior surface was an area weighted average of the emissivities of ACC and aluminium (67% x 0.85 + 33% x 0.095 = 0.60) [24] [25]. The heat input to the coil was related to the LTJ test

$$Q_{coil}(t) = m_x \Delta X^* h_{fg} \left(1 - \exp\left(-\frac{\tau_{1/2}}{\tau_{(a-lx)}}\right)\right) \qquad [15]$$

where h_{fg} is the specific heat of vaporisation.

Certain radial profiles of temperature were established to obtain (1) average fin temperatures used in the energy storage terms (2) the fin tip temperatures for heat losses (3) the heat losses through the brass plug at the base of the generator. The one dimensional equations for thermal conduction in either the idealised fins or brass plug were:

$$\rho\, c_p\, \frac{\partial T}{\partial t} = \frac{\dot{Q}_{fin}}{V} + \frac{\lambda}{r}\, \frac{\partial}{\partial r}\left(r\, \frac{\partial T}{\partial r}\right) \qquad [16]$$

276

277 where ρ is fin (or plug) density, V is the volume of the flanks and Q_{fin} is the rate of heat transfer to the
278 fin flanks, estimated as $\delta Q_{fin} = \delta Q^{(a\text{-}lx)}$ for fins and $\delta Q_{fin} = 0$ for the brass plug. For conjugate heat
279 transfer at $r = d_{HX}/2$ the boundary condition was,

$$\frac{\partial T(r = \frac{d_{HX}}{2})}{\partial r} = -\frac{\alpha}{\lambda}\, F\left(T_s - T\left(r = \frac{d_{HX}}{2}\right)\right) \qquad [17]$$

280

281 where subscript HX refers to the outer diameter of the heat exchanger, subscript s refers to the heat
282 transfer liquid, and F is a geometric factor taken as F = 1 for the brass plug or F =13, the ratio of fin
283 spacing to fin thickness. The heat transfer coefficient was estimated, as appropriate, from either
284 Nusselt film theory or the Dittus-Boelter equation. (Perfect contact between tube and fin was
285 assumed.)

286 The estimated (isothermal) temperature of the glass cover was

$$T_{cover}(t) = T_{cover}^{start} + \frac{U_{cover} A_{cover} \int_{start}^{t} \left(T_{amb} - T_{glass}(t)\right) dt' + Q_{HT}}{m_{cover}\, c_{glass}} \qquad [18]$$

287

288 where the heat transfer term Q_{HT} is equal to the convective and radiative loss parts of Equation 9.

289 The performance parameters were,

290

$$COP = \frac{Q_{coil}(evap)}{Q_{in}\,(heating)} \quad [19]$$

$$SCP = \frac{Q_{coil}(evap)}{2\,m_x\,\tau_{1/2}} \quad [20]$$

where SCP represents the average specific cooling power, that is the cooling effect (Q_{coil}) per unit mass of adsorbent (m_x) per unit time (2 $\tau_{½}$).

4. Results

This section reports temperatures and pressures measured during the refrigeration cycle, the energy balance, and the chiller performance in terms of COP and SCP.

Fig. 7 compares the cycle with a hypothetical quasi-equilibrium cycle (drawn in bold as a near parallelogram). The temperature measurement was on the mid-plane of the ACC and lagged behind the temperature of working fluid, so that spatially averaged ACC temperature would have been greater than indicated during the heating processes and less than indicated during the cooling processes. The two horizontal isobars on the hypothetical cycle correspond to saturation pressures calculated from the temperatures of the evaporator load (273 K) and condenser sink (293 K). Temperature differences as high as 273 – 265 = 8 K were required to drive heat transfer to the evaporator and similarly for the condenser.

Fig. 8 presents temporal plots of refrigerant pressures. Following temporary application of *vacuum* the pressure in the isolated generator had decreased from 60 to 39 mbar. The non-linear adsorption relationship (Equation 5) indicated that the capacity would have changed slightly from X* = 0.398 to X* = 0.387. Up to time t < 100 s, the condenser held a pressure of 72 mbar - the saturation pressure at the temperature of the condenser sink. Subsequently heating the generator and then connecting it to the condenser caused the pressures in both to surge. During vapour adsorption / evaporation (t > 1920 s), saturation temperatures of the refrigerant, labelled 5°C and 18°C on part (b), were somewhat less than the temperature of the evaporator load confirming the requirement for an appreciable temperature driving force.

A delay of ~120 s applied after the opening of the evaporator valve (t = 1920 s); the temperature of the evaporator load lagged the evaporator pressure. This might be due to the dynamics aspects of the evaporator, for example a 3.3-mm thick ethanol layer would have a characteristic conduction time of 120 s.

Fig. 9 shows measured and predicted temperatures for three parts of the generator. The fin tip and the brass plug did not quite, as expected, meet the steam temperature. The root mean square errors for heating and cooling phases, labelled e_{rms} on each part of Fig. 9, would have led to discrepancies in the estimated convective and radiative heat loss from the adsorption heat exchanger (corresponding to 4% of the heat supplied by the exchanger and 8% of the heat removed). Any deviation from the conditions for LTJ (a step change in temperature at the fin root) might explain the prediction anomalies at the positions labelled 'P' and 'Q'.

Thermocouples could not be installed at the fin root during manufacture. Nonetheless, the temperatures measured in the ACC mid-plane indicate that the temperature change at the fin root was not instantaneous (that is, associated thermal resistances were appreciable). The ACC cooled more slowly than during the smaller-scale LTJ tests (Fig. 10). Admittedly the fin shape and the co-ordinates of thermocouples differed, but after 100s predicted axial temperature gradients along the fins for both LTJ tests and the adsorption heat exchanger were < 1 K [11]. (Thermocouples were in the centre of a square mid-plane for LTJ tests but within 3 mm of the edge for the adsorption heat exchanger). The differences between ACC temperatures within the adsorption heat exchanger could be due to (1) different orientation of thermocouples at the three locations, or even possible penetration of beads through layers of cloth during manufacture and pressing of the bed (2) different compression of the bed at different locations, associated with manufacturing tolerances (3) localised crumpling of fabric during manufacture.

The energy balance compared net heat inputs to the generator (during desorption) with net heat outputs (during adsorption). Considering the heating process alone, 16% of heat added to the generator was used to desorb ethanol, evident as heat transfer to the condenser sink plus the estimated heat of phase change (typical experiment, Table 3). A larger amount, 61% of heat addition, appeared

as changed sensible heat in infrastructure. (Appendix A gives the justification for uncertainties in Table 3, computed from known instrument errors and uncertainties in material properties. The overall theoretical uncertainty in total heat input was 6 %. The discrepancy of 13% between heat input and balancing terms in Equation 7 was a better indication of accuracy.)

Table 4 shows coefficient of performance, specific cooling power and the characteristic time for cooling of the evaporator load (τ_{adiab}). Cooling was slower than expected from the smaller scale tests; the characteristic time was $\tau_{adiab} \in [189, 409]$s, versus $\tau_{(a\text{-}lx)} \in [159, 189]$s [11]. The possible slower temperature change of the fin root has already been mentioned. In addition there may be heat transfer resistances in the evaporator, resulting initially in reduced refrigerant temperatures (for instance the labelled saturation temperature of 5°C (p = 21 mbar) on Figure 8). However, any impact on adsorption rate is mitigated by the non-linearity of the isotherm. For example (with adsorbent held at 30 °C) a vapour pressure p = 21 mbar (T_{sat} = 5°C) gives X^* = 0.341 whereas at p = 51 mbar (T_{sat} = 18°C) X^* = 0.386 (from Equation 5). Thermal resistance at the fin root is the governing heat transfer resistance, although mass transfer might also be important and in particular Glaznev et al [26][27] measured a 40% change in rate of moisture adsorption with partial pressure of air as low as 0.06 mbar on 10 mbar total pressure. (They considered moisture adsorbed by silica gel, FAMZ02 and SWL-1L.) The effect on desorption was noticeable but less severe. They contemplated Stefan flows and the production of an inert gas film at the grain external surface, albeit as one of several complex, coupled processes.

362 **Table 3 Typical heat balance**

363

	Heating		**Cooling**		
	kJ	error, %	kJ	error,%	Comment
Desorption					
Condenser sink	82	±14%			Sensible energy in Eqn 7, Eqn A.4
Phase change	2	±32%			Phase change in Eqn 7
Sub total (*% grand total)*	84 (16%)	±14%			Error from Eqn A.1
Adsorption					
Evaporator load	-		-107	±7%	Sensible energy in Eqn 7, Eqn A.4
Phase change	-		3	±32%	Phase change in Eqn 7
Sub total (% grand total)			-104 (29%)	±7%	Error from Eqn A.1
(Generator)					
ACC (dry)	43	±8%	-44	±9%	Sensible energy in Eqn 7, Eqn A.4
EtOH (sorbed)	11	±8%	-9	±9%	Sensible energy in Eqn 7, Eqn A.4
Fins (Al)	37	±3%	-31	±3%	Sensible energy in Eqn 7, Eqn A.4
HX (Cu)	21	±3%	-19	±3%	Sensible energy in Eqn 7, Eqn A.4
Cover (glass)	128	±11%	-104	±11%	Sensible energy in Eqn 7, Eqn A.4
Plug (brass)	82	±7%	-73	±7%	Sensible energy in Eqn 7, Eqn A.4
Sub total (*% grand total)*	322 (61%)	±5%	-280 (78%)	±5%	Error from Eqn A.1
Direct Losses (Generator)					
Cover (glass)	37	±30%	27	±30%	Direct loss in Eqn 7, Eqn A.6
Brass Plug	5	±30%	4	±30%	Direct loss in Eqn 7, Eqn A.6
Sub total (% grand total)	42 (8%)	±27%	31 (-9%)	±26%	Error from Eqn A.1
External Pipework					
Sensible Heat	62	±30%	-8	±30%	Direct loss in Eqn 7, Eqn A.6
Direct Loss	15	±30%	4	±30%	Direct loss in Eqn 7, Eqn A.6
Sub total (% grand total)	77 (15%)	±25%	-4 (1%)	±22%	Error from Eqn A.1
Grand total	**525**	±6%	**-358**	±4%	
Applied heat transfer					
Steam	**602**	±4%			
Cooling water			**-452**	±9%	Sensible energy in Eqn 7, Eqn A.4
Discrepancy	-13%		21%		Grand total - Applied heat transfer
COP	17.8%	±9%	Eqn 14, Eqn A.2		
SCP, kW/ kg(ACC)	0.071	±7%	Eqn 15		

364

365 NB: Methodology for uncertainty analysis is given in appendix A

Table 4 Impact of operating condition on measured and predicted performance

	COP x 100 - Measured	COP x 100- Adjusted scaling Eqn 11, 19	COP x 100- Simple scaling Eqn 10, 20	SCP, W kg^{-1} Measured	SCP, W kg^{-1} Predicted	τ_{adiab}, s
Impact of cycle time, T_{re}= 288 K , T_{rc} = 302 K						
Cycle time, mins						
2 x 10	23.6±2.3	22.3	46.8	126±15.9	181	180
2 x 20	22.0±2.5	30.7	47.4	71± 8.4	93	254
2 x 30	21.3±1.6	27.5	45.9	53±10.7	59	199
Impact of condenser temperature, t_{cycle} = 2 x 20 mins, T_{re} = 288 K				-		
T_{rc}, K						
299	19.0±0.4	30.2	46.6	62±6.5	89	228
309	15.5±0.6	25.2	44.4	49±1.6	72	313
319	11.9±0.1	26.0	38.9	36±6.3	72	202
Impact of evaporator temperature, t_{cycle} = 2 x 20 mins, T_{rc} = 290 K						
T_{re}, K						
268	17.6	28.1	39.7	54	85	295
277	20.1	31.0	40.6	62	98	409
287	16.5	29.9	45.6	55	89	183

T_{re} = temperature of refrigerant in evaporator coil

T_{ce} = temperature of refrigerant in condenser coil

"Ideal" estimate neglects sensible heat of cover (glass) and plug (brass)

Uncertainties are standard deviations from three repeat experiments (when available)

377 Three versions of COP are presented in Table 4: direct measurement; the adjusted scaling
378 procedure (Equations 11, 19), and simple scaling (Equations 10, 20). When the impact of cycle time
379 was probed COPs from the simpler scale up procedure varied slightly owing to variations in
380 generator/ condenser pressure. The durations of half-cycles were at least 3.3 times greater than the
381 characteristic time for evaporator load cooling (column *7 of* Table 4), so the minimal impact of cycle
382 time on COP is unsurprising. The simpler scale up exceeded the measured COP by a factor of 2 to
383 2.8. For the adjusted scale up the factor of error (in COP) ranged from 1.0 to 1.6. For SCP, the range
384 is 1.1 to 2.0; this compares with 2 to 6 elsewhere [8] although the discrepancy is attributed largely to
385 the heat capacity of metal supports and differing thicknesses of adsorbent layer. Some impact of
386 temperature lift is evident from changes in evaporator and condenser temperature.

387

388 **5. Further Discussion**

389 The discrepancy in the heat balance and the uncertain influence of air ingress justifies a
390 scale-up method, rather than detailed mechanistic models. In future the control mechanism and
391 boundary conditions for small-scale tests should: (1) mimic thermal resistances at the fin root, rather
392 than a strict step change in temperature (LTJ); (2) deal with a controlled ingress of air or inert gas; (3)
393 employ boundary conditions that mimic direct solar illumination.

394 The machine performance is compared against three other pieces of work (Table 5). The
395 COP is more favourable than achieved elsewhere with granular carbon [28]. Better COP was achieved
396 with Methanol [29]; it offers a higher heat of vaporisation and a higher adsorption capacity. The
397 maximum measured loading on Chemviron ACC was 44% [30] versus 35% for ethanol. (Litre
398 quantities of methanol were avoided in our laboratory owing to its toxicity.) Alternatively, water has
399 the highest heat of vaporisation [31], and tests with silica gel beads show comparable characteristic
400 times to those reported here [32]. Better COP was also achieved with larger AHPs (9 kW cooling
401 power) [31]. (Larger scale offers comparatively less dynamic and steady heat loss per unit mass of
402 adsorbent.)

403

404

405

406

407 ***Table 5 Performance of Several AHPs***

Author	Pair used	SCP, W kg^{-1}	COP (thermal)	*Conditions*
Current work	AC-EtOH	59 to 181	0.119 to 0.236	*Adsorbing/ desorbing time 10 to 30 minutes, heating temperature 100°C, evaporator temperature 268 to 287 K*
Liu et al [28]	ACC-EtOH		0.029 to 0.034	*Desorbing time 6 hrs, Adsorbing time 18 hours load temperature reduced from 20°C to 4°C, 14.6 to 19.4 MJ irradiation (accepted)*
Liu et al [28]	ACC-MeOH		0.105 to 0.113	*As above*
Boubakri et al [29]	ACC-MeOH		0.295 to 0.339	*Ice making, hence load at 0°C. Collector temperature 26 to 100°C over 10 hours.*
Liu et al [31]	Silica gel-water	341	0.15 to 0.40	*Temperatures 70°C to 95°C. Cooling water inlet temperatures 24 to 34°C. Evaporating temperature 5 to 16°C. Heat and mass recovery possible.*

408

409

410

411

412 The impact of air ingress on adsorption is complex. In principle very small mole fractions of

413 air (~0.1%) can create large reductions in rate of adsorption. If one considers only mass transfer to the

414 faces of the adsorbent heat exchanger, then for Stefan flows [33] the mole fraction of ethanol, y,

415 changes according to

$$1-y_{\delta}=(1-y_0)\exp\left(\frac{u_{face}\delta}{D}\right) \qquad [16]$$

where u_{face} is the face velocity, δ is the boundary layer thickness, D is the molecular diffusivity of ethanol in air, and subscripts 0 and δ indicate mole fractions on either side of the boundary layer. A worked example yields $u_{face}\,\delta/D = 6.4$ and $y_o = 99.9\% \rightarrow y_\delta = 60\%$ so that marked reductions in ethanol mole fraction are conceivable (change in adsorption capacity, $\Delta X^* = 20\%$, characteristic time $\tau_{adiab} = \tau^{(a-lx)} = 200s$, and boundary layer thickness, $\delta = 3$ mm). The exponential function is highly sensitive to local boundary layer thickness and face velocity so that y_δ cannot be quantified with precision; it could be far greater or far less than 60%. A further complication is any air ingress in the pipe from evaporator to adsorber. The length scale is far greater (L = 1.8 m vs $\delta \sim 3$ mm) although longitudinal dispersion should also come into play provided flow is turbulent. This is not captured well in scale up from the smaller experiments. Even assuming sample and full-size beds are subject to the same boundary conditions, the initial velocities would be about six times higher in the pipe of the full scale generator (where the adsorbent mass is 60 times higher but the tube cross sectional area only 10 times higher). On the other hand, the pipe in the smaller rig is only 30 cm long (versus 1.8 m). Furthermore air ingress between ACC fibres is possible, and interaction between oxygen and the functional groups in the ACC is conceivable . The net effect is to slow the adsorption rate possibly to such an extent that full adsorption capacity is not reached in realistic time. This explains differences in the scale up of both coefficient of performance and cooling power.

Solar testing is planned for future work. This requires elevating a concentrating mirror by a further 2m above the base of the generator and hence some construction work. A more subtle problem is simulating irradiation boundary conditions in the calorimeter. An interesting and challenging aspect will be the response of the integrated generator/ collector to cloud cover.

Equation [10] is related to the predictive technique, where one might expect some ultimate benefit to the designer from a non-dimensional approach. But, for the purposes of the current paper, caution is advised for two reasons. (1) Seminal work using LTJ on comparatively large samples was presented in references [8], [9] [10]. At no stage were non-dimensional groups mentioned here. (2) A necessary condition is dimensional similarity; it is not clear that this condition would be

retained. A critical ratio of dimension is that fin-to-fin gap divided by fibre diameter which in present studies was identical at bench scale and full scale.

The AHP could be better optimised in future. A set of tests on fins with different fin-to-fin gaps is planned at small scale. The samples have been wire cut with gaps as small as 1-mm, although manufacture of such fins will be problematic for full-scale AHPs. Other improvements are (1) use of methanol as a refrigerant (2) screening of carbon cloths for best adsorption properties (3) larger adsorption heat exchangers (4) reduction of heat losses to the cover (in particular the plug should be replaced with a thermal insulator) (5) restricting the aperture size for the glass cover, and double glazing the rest of the cover (6) the use of carbon adsorbents with enhanced thermal conductivity, e.g. carbons mixed with expanded natural graphite. The use of two-axis solar tracking would permit a far smaller optical aperture [34]. Future testing with a solar simulator is essential - however even with a "low cost" design the expense was $10 000 for focussing xenon lighting to 45 kW m^{-2} on a 38-mm-diameter target [35], roughly the concentration factor needed for our experiments. Halogen lamps would reduce cost many times and illuminate the entire target area (but would not replicate the power spectrum of natural sunlight).

6. Conclusions

A laboratory scale AHP has integrated the roles of adsorbent bed, heat exchanger and solar collector. For the first time, a scale up procedure has been applied to calorimetric LTJ tests. For the conditions tested the values of COP were 1.0 to 1.6 times less than those expected by scaling-up data from smaller samples. The SCP was 1.6 to 2.0 times less than expected compared with factors of discrepancy of 2 to 6 elsewhere. It is hypothesised that even very small levels of air ingress ($y < 0.1\%$) influenced results.

Given the uncertain influence of air ingress and the quality of the heat balance (to 15%) detailed mechanistic models are not recommended at this stage of our work. The existing analysis allows areas of improvement to be identified in future designs (1) mitigation of dynamic losses, and in

particular the replacement of a brass sealing plug (2) use of methanol as a refrigerant (3) optimisation of fin spacing.

ACKNOWLEDGEMENT

The authors acknowledge funding from the Leverhulme Trust under grant reference F00182CD.

REFERENCES

[1] B. N. Okunev, A. P. Gromov, L. I. Heifets, Y. I. Aristov, A new methodology of studying the dynamics of water sorption/desorption under real operating conditions of adsorption heat pumps: Modelling of coupled heat and mass transfer in a single adsorbent grain, Int. J. Heat Mass Transfer 51(1) (2008), 246-252.

[2] A. Rezk, R. K. Al-Dadah, S. Mahmoud, A. Elsayed, Effects of contact resistance and metal additives in finned-tube adsorbent beds on the performance of silica gel/water adsorption chiller. Appl. Therm. Eng.,53(2) (2013) 278-284.

[3] S. D.Waszkiewicz, M. J.Tierney, H. Saidani-Saidani-Scott, Development of coated, annular fins for adsorption chillers, Appl. Therm. Eng. 29(11) (2009) , 2222–2227.

[4] R. E.Critoph, Y. Zhong, Review of trends in solid sorption refrigeration systems, J. Proc Mech. Eng., 219 (3) (2005), 285-300.

[5] R.Z.Wang, Adsorption refrigeration research in Shanghai Jiao Tong University, Renewable and Sustainable Energy Reviews, 5(1) (2001), 1-37.

[6] K. Sumathy, K. H.Yeung, L. Yong, Technology development in the solar adsorption refrigeration systems, Progress in Energy and Combustion Science, 29(4) (2003), 301-327.

[7] L. W. Wang, Z.Tamainot-Telto, R.Thorpe, R. E. Critoph, S. J. Metcalf, R. Z. Wang, Study of thermal conductivity, permeability, and adsorption performance of consolidated composite activated carbon adsorbent for refrigeration, Renewable energy 36(8) (2011) 2062-2066.

[8] Y. I Aristov, I. S. Glaznev, I. S. Girnik, Optimization of adsorption dynamics in adsorptive chillers: Loose grains configuration, Energy 46 (1) (2012) 484-492.

[9] S. Sapienza, S. Santamaria, A. Frazzica, A. Freni, Y. I. Aristov, Dynamic study of adsorbers by new gravimetric version of the Large Temperature Jump Method, Appl. Energy 113 (2014) 1244-1251.

[10] S. Santamaria, A. Sapienza, A. Frazzica, A. Freni. I. Girnik, Y.I. Aristov, Water adsorptive dynamics on representative pieces of real absorbers for adsorptive chillers, Appl. Energy 134 (2014) 11-19.

[11] M. Tierney, L. Ketteringham, R. Selwyn, H.Saidani, Calorimetric measurements of the dynamics of a finned adsorbent: early assessment of the activated carbon cloth–ethanol pair with prismatic aluminium fins, Appl. Thermal Engineering, 93 (2016), 1264-1272.

[12] https://www.corning.com/media/worldwide/csm/documents/71759a443535431395eb34ebead091cb.pdf (accessed 18/05/2016)

[13] M. A. Ahamat, M. J. Tierney, Timewise temperature control with heat metering using a thermoelectric module, Appl. Therm. Eng., 31 (2011), 1421-1426.

[14] B. N.Okunev, A. P.Gromov, L. I., Heifets, Y. I. Aristov, Dynamics of water sorption on a single adsorbent grain caused by a large pressure jump: Modeling of coupled heat and mass transfer, Int. J. Heat Mass Transfer 51(25) (2008) 5872-5876.

[15] I.I. El-Sharkawy, K. Kuwahara, B. B. Saha, S. Koyama, K. C. Ng, Experimental investigation of activated carbon fibers/ ethanol pairs for adsorption cooling system application. Appl. Therm. Eng. 26 (2006) 859-865.

[16] I.I. El-Sharawy, K. Uddin, T. Miyazaki, B. B. Saha, S. Koyama, H Kil, S Yoon, J. Miyawaki, Adsorption of ethanol onto phenol resin based adsorbents for developing next generation cooling systems. Int. J. Heat and Mass Transfer 81 (2015) 171-178

[17] V. Brancato, A. Frazzica, A. Sapienza, L. Gordeeva, A. Freni, Ethanol adsorption onto carbonaceous and composite adsorbents for adsorptive cooling system. Energy 84(1),(2015),177-185.

[18] R. E. Critoph Performance limitations of adsorption cycles for solar cooling. Solar Energy 41(1), (1988), 21-31.

[19] A. Chakraborty, B. B. Saha, K. C. Ng, S. Koyama, K. Srinivasan, Theoretical insight of physical adsorption for a single component adsorbent + adsorbate system: I. thermodynamic property surfaces. Langmuir, 25 (2009) 2204-2211.

[20] A. Chakraborty, B. Sun, An adsorption isotherm equation for multi-types adsorption with thermodynamic correctness. Appl. Therm. Eng., 72, (2014), 190-199.
[21] A. Chakraborty, Thermodynamic trends for the adsorption of non polar gases on activated carbons employing a new adsorption isotherm modelling. Appl. Therm. Eng., 105 (2016) 189-197.
[22] A. J. Chapman, Heat Transfer, fourth ed., MacMillan, New York, 1984
[23] S. W. Churchill, H. H. S. Chu, Correlating equations for laminar and turbulent free convection from a vertical plate, Int. J. Heat Mass Transfer, 18(11) (1975) 1323-1329.
[24] J. R. Howell, R. Siegel, M. Pinar Menguc. Thermal radiation heat transfer. CRC press, New York, 2010.
[25] P.Coss, A. Moses, and Y. C. Chang, Microwave regeneration of activated carbon used for removal of solvents from vented air, J. Air & Waste Management Association 50(4) (2000) 529-535.
[26] I.Glaznev, D. Ovoshchnikov, Y. Aristov, Effect of residual gas on water aadsorption dynamics under typical conditions of an adsorption chiller, Heat Transfer Engineering 31 (11) (2010) 924- 930.
[27] I. S. Glaznev, and Y. I. Aristov, Kinetics of water adsorption on loose grains of SWS-1L under isobaric stages of adsorption heat pumps: the effect of residual air, Int. J. Heat and Mass Transf. 51(25) (2008) 5823-5827.
[28] M. Liu, H. B. Huang, R. Z. Wang, L. L. Wang, W. D. Cai, W. M. Yang, Experimental study on adsorbent of activated carbon with refrigerant of methanol and ethanol for solar ice maker, Renewable Energy 29(15) (2004) 2235–2244.
[29] A. Boubakri, J. J. Guilleminot, F. Meunier, Adsorptive solar powered ice maker: experiments and model, Solar Energy 69(3)(2000) 249–263.
[30] Fan Yin, Measurement of parameters for design of adsorption chiller, Thesis (Ph.D.), University of Bristol 2013.
[31] Y. L. Liu, R. Z. Wang, and Z. Z. Xia, "Experimental performance of a silica gel–water adsorption chiller," Appl. Therm. Eng., 25(2-3)(2005) 359–375.
[32] M. A. Ahamat, M. J. Tierney, Calorimetric assessment of adsorbents bonded to metal surfaces: application to type A silica gel bonded to aluminium, Appl. Therm. Eng. 40 (2012) 258-266.
[33] J. M. Coulson, J. F. Richardson, , J. R.Backhurst, J. H. Harker, Vol. 1: Fluid flow, heat transfer and mass transfer. Butterworth Heinemann, Oxford ,1996.
[34] M. Tierney, L. Ketteringham, R. Selwyn, M. Ahamat, H. Saidani, An adsorption heat pump with concentrating solar collector: concept design, Proc. Int. Sorption Heat Pump Conference, Curran Associates, New York (2014), 397-405.
[35] D. S. Codd, A.Carlson, J. Rees, A. H. Slocum,. A low cost high flux solar simulator. Solar Energy, 84(12) (2010) 2202-2212.

479

480

481

482

483

LIST OF FIGURES

Fig. 1 The experiment proper: 1. Heat exchanger (annulus tube) 2. Glass dome 3. ACC bed 4. Heat exchanger inlet/outlet 4a. Brass plug 5 Isolation valve from generator 6. Isolation valves between condenser and evaporator 7. Valve – to vacuum pump 8. Drain/ fill valve 9. Pressure transducers 10. Condenser heat sink 11. Condenser coil 12. Ethanol sight tube 13. Evaporator heat load 14. Evaporator coil 15. Cooling water inlet (also used as steam outlet) 16. Steam inlet/ cooling water outlet (also used as steam inlet) 17. Fin (•) Thermocouple location

Fig. 2 Arrangement used to establish data (a) line drawing (b) photograph of essential items of interest. Items (1) thermoelectric module (TEM) (2) thermocouple locations (3) fin (4) fin gap - ACC filled (5) vessel casing. ***Reprinted from Applied Thermal Engineering,vol. 93, M. Tierney et al. , Calorimetric Assessment of the Dynamics of a Finned Adsorbent. Copyright 2016, with permission from Elsevier.***

Fig. 3 Data from small AdHex samples (a) heat rejection as a response to LTJ, dotted lines show fits to $Q^{(a\text{-}lx)}$ and $Q^{(a\text{-}l)}$ and confirm exponential trends. Conditions are listed in row 2 in Table 1 (b) adsorption capacity. Reprinted from Applied Thermal Engineering, vol. 93, M. Tierney et al. , Calorimetric Assessment of the Dynamics of a Finned Adsorbent. Copyright 2016, with permission from Elsevier.

Fig. 4 Estimated heat rejection versus measured value for bench scale tests (■ LPJ tests, ▲ LTJ*).*

Fig. 5 Abstract view of experiment, giving closed system boundary for thermal measurement (1) boundary of closed system (2) cover (glass) (3) plug (brass) (4) AdHex (5) steam supply) (6) condenser heat sink (7) condenser coil (8) cold water supply (9) evaporator cooling load (10) evaporator coil (11) pipework.

Fig. 6 Analysis of evaporator load temperature. Point A is start of evaporation, point B is suspected cessation of evaporation, curve ABC is raw data, curve ADE has been corrected to estimate an adiabatic load (using temperatures from BC), curve AF is fitted to AD and extrapolated($r^2 = 0.9972$ and $\tau_{adiab} = 254$ s)

Fig. 7 Clapeyron plot of generator pressure versus ACC temperature. Cycle time = 20 minutes, the evaporator heat load is at 273 K and the condenser heat sink is at 293 K. The processes are (1)-to-

(2) heating of the bed at near constant loading, (2)-to-(3) desorption of ethanol from the bed and condensation, (3)-to(4) cooling of the bed at constant loading, (4)-to-(end) adsorption of ethanol into the bed and evaporation (producing refrigeration). The bold lines show a quasi-equilibrium cycle.

Fig. 8 Development of refrigeration pressures and impact on the evaporator load (a) pressures in the three main parts of the chiller (b) temperature of the evaporator load. The refrigerant temperatures, labelled on part (b), were calculated from evaporator pressures on part (a).

Fig. 9 Selected temperatures in the generator throughout a cycle. (a) fin tip (item 17 on Fig. 1) (b) glass cover (item 2 on Fig. 1) (c) brass plug. Dots represent measured data and thin solid lines predictions.

Fig. 10 Temperatures measured in the ACC mid-plane. Temperatures measured under LTJ are plotted for comparison using the right hand y-axis, starting at time = 1000 s approximately. Thermocouple positions are shown as item #18 in Fig. 1 and item #2 in Fig. 2.

List of Tables

562

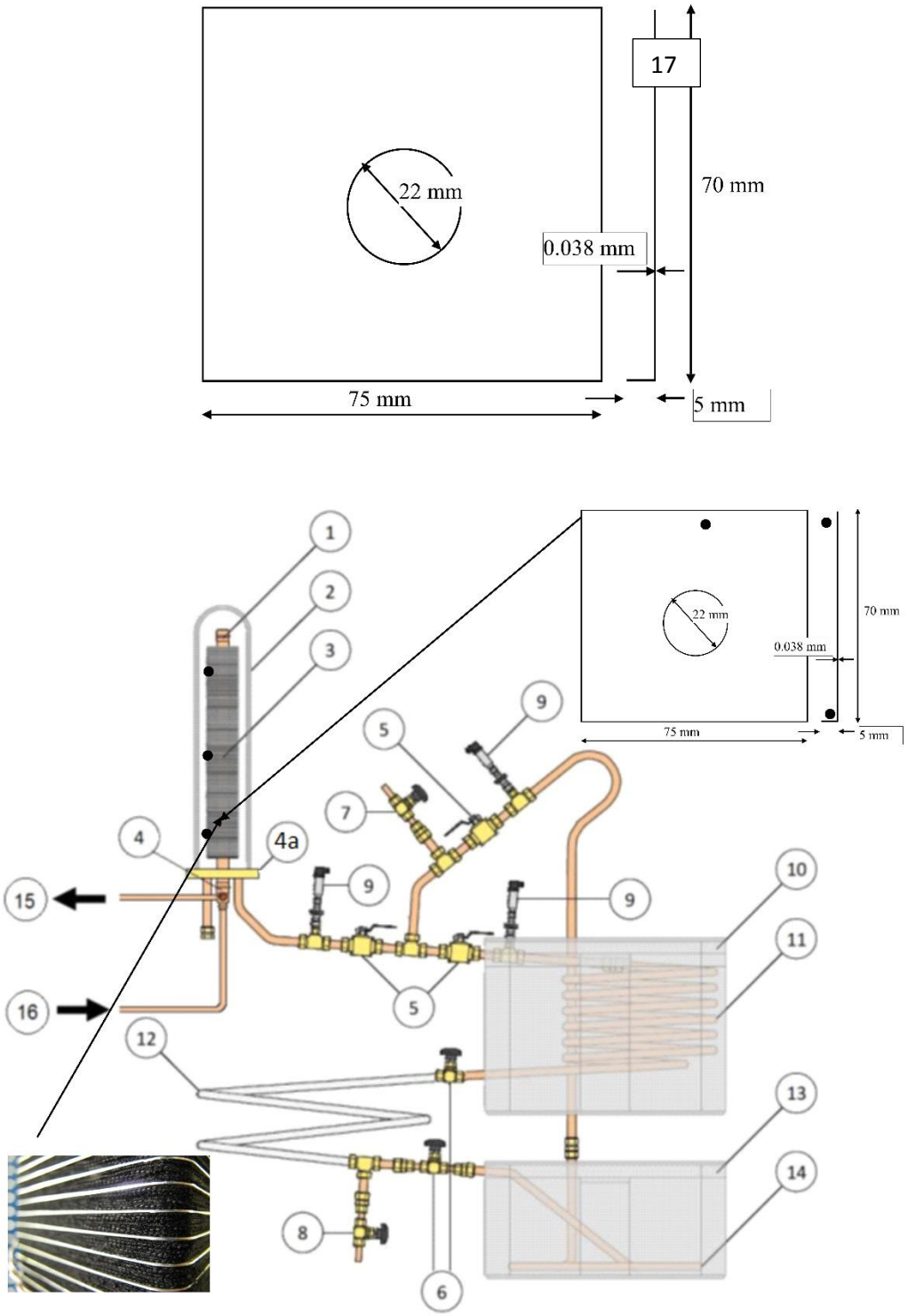

563

564 **Fig. 1: The experiment proper: 1. Heat exchanger (annulus tube) 2. Glass dome 3. ACC**
565 **bed 4. Heat exchanger inlet/outlet 4a. Brass plug 5 Isolation valve from generator 6.**
566 **Isolation valves between condenser and evaporator 7. Valve – to vacuum pump 8.**
567 **Drain/ fill valve 9. Pressure transducers 10. Condenser heat sink 11. Condenser coil**
568 **12. Ethanol sight tube 13. Evaporator heat load 14. Evaporator coil 15. Cooling water**
569 **inlet (also used as steam outlet) 16. Steam inlet/ cooling water outlet (also used as steam**
570 **inlet) 17. Fin (•) Thermocouple location**

571

572

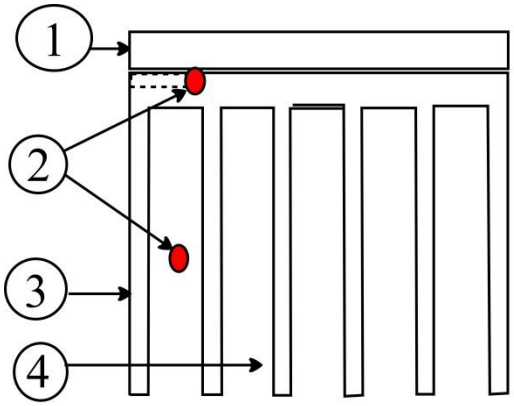

573

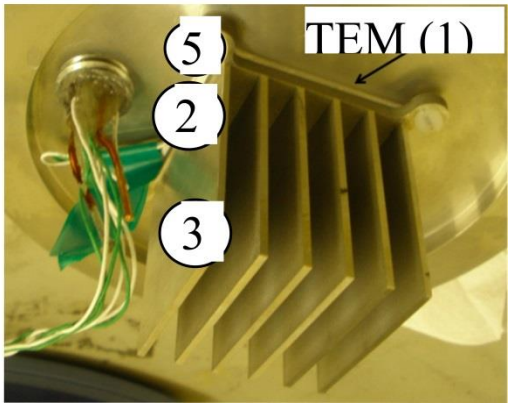

574

575 (a) (b)

576

577 **Fig. 2 Arrangement used to establish data (a) line drawing (b) photograph of essential items of**
578 **interest. Items (1) thermoelectric module (TEM) (2) thermocouple locations (3) fin (4) fin gap -**
579 **ACC filled (5) vessel casing.** ***Reprinted from Applied Thermal Engineering,vol. 93, M. Tierney et***
580 ***al. , Calorimetric Assessment of the Dynamics of a Finned Adsorbent. Copyright 2016, with***
581 ***permission from Elsevier*.**

582
583

584

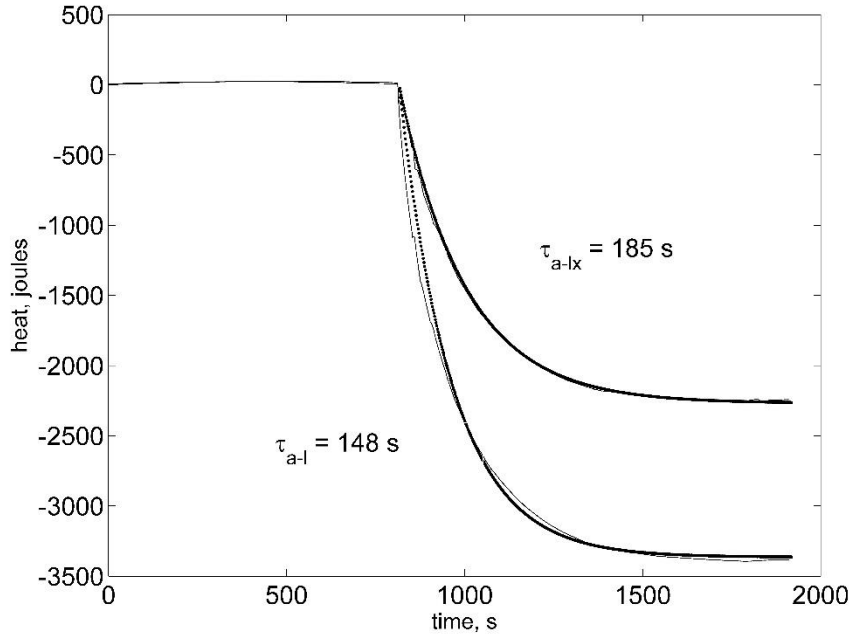

(a)

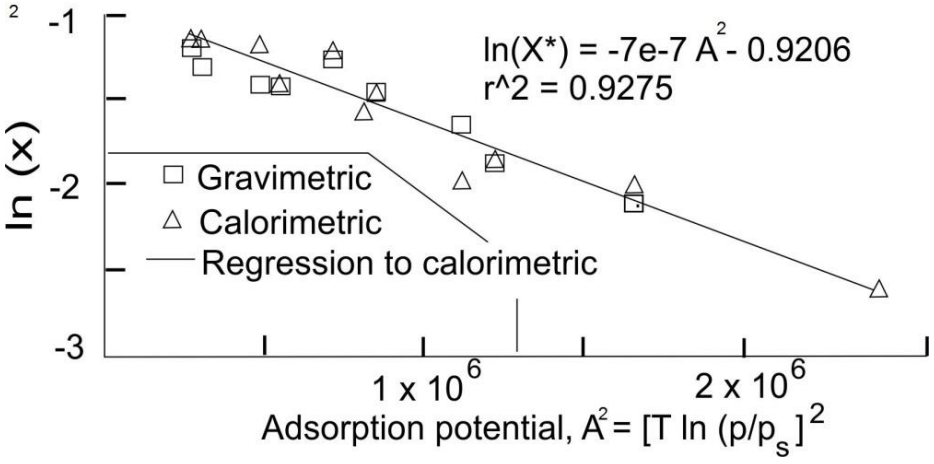

(b)

Fig. 3 Data from small AdHex samples (a) heat rejection as a response to LTJ, dotted lines show fits to $Q^{(a-lx)}$ and $Q^{(a-l)}$ and confirm exponential trends. Conditions are listed in row 2 in Table 1 (b) adsorption capacity. ***Reprinted from Applied Thermal Engineering, vol. 93, M. Tierney et al. , Calorimetric Assessment of the Dynamics of a Finned Adsorbent. Copyright 2016, with permission from Elsevier.***

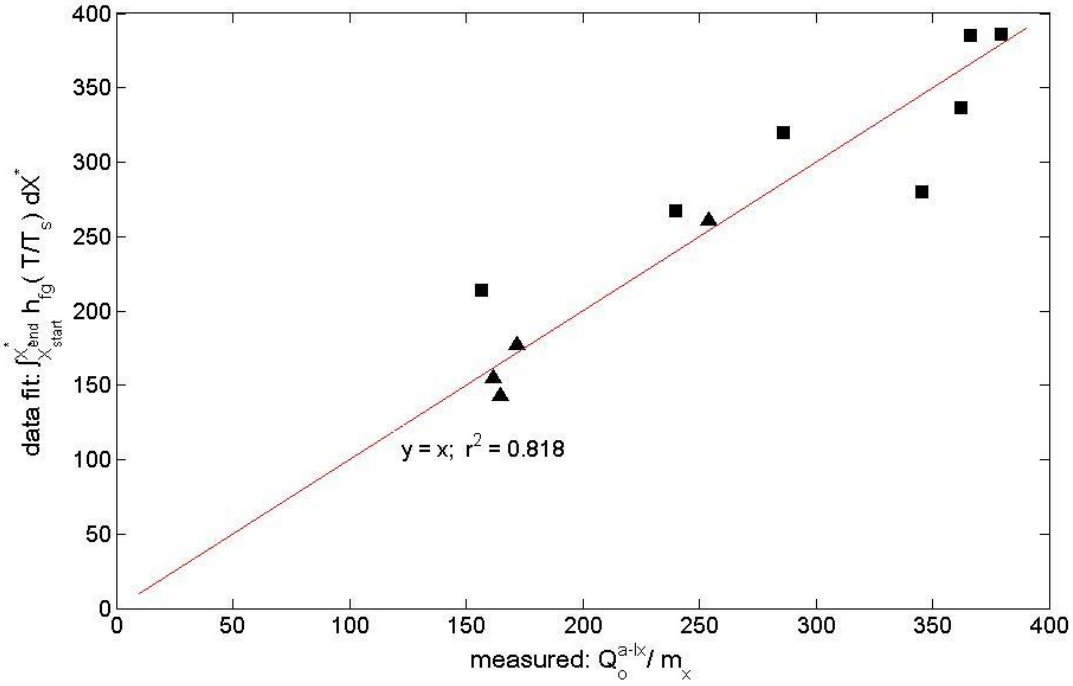

598

599 **Fig. 4 Estimated heat rejection versus measured value for bench scale tests (■ LPJ tests, ▲**

600 **LTJ)**

601

602

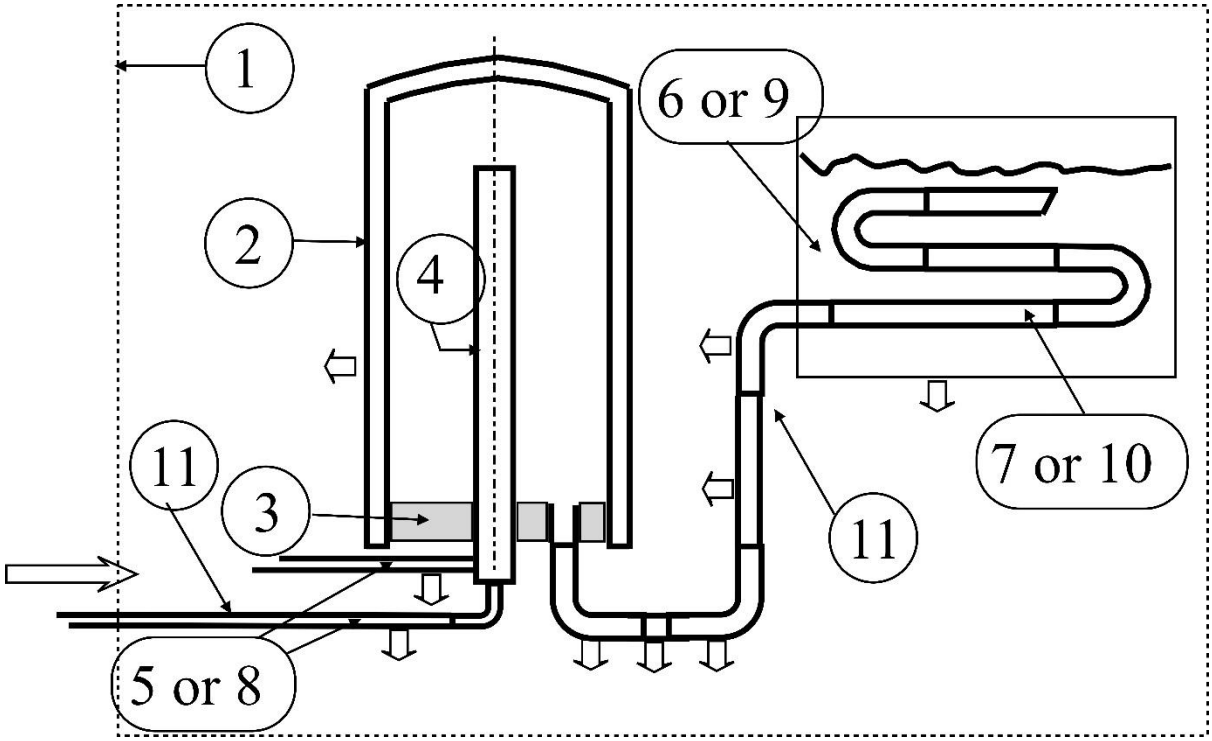

603

604

605 **Fig 5. Abstract view of experiment, giving closed system boundary for thermal measurement**
606 **(1) boundary of closed system (2) cover (glass) (3) plug (brass) (4) AdHex (5) steam supply) (6)**
607 **condenser heat sink (7) condenser coil (8) cold water supply (9) evaporator cooling load (10)**
608 **evaporator coil (11) pipework.**

609

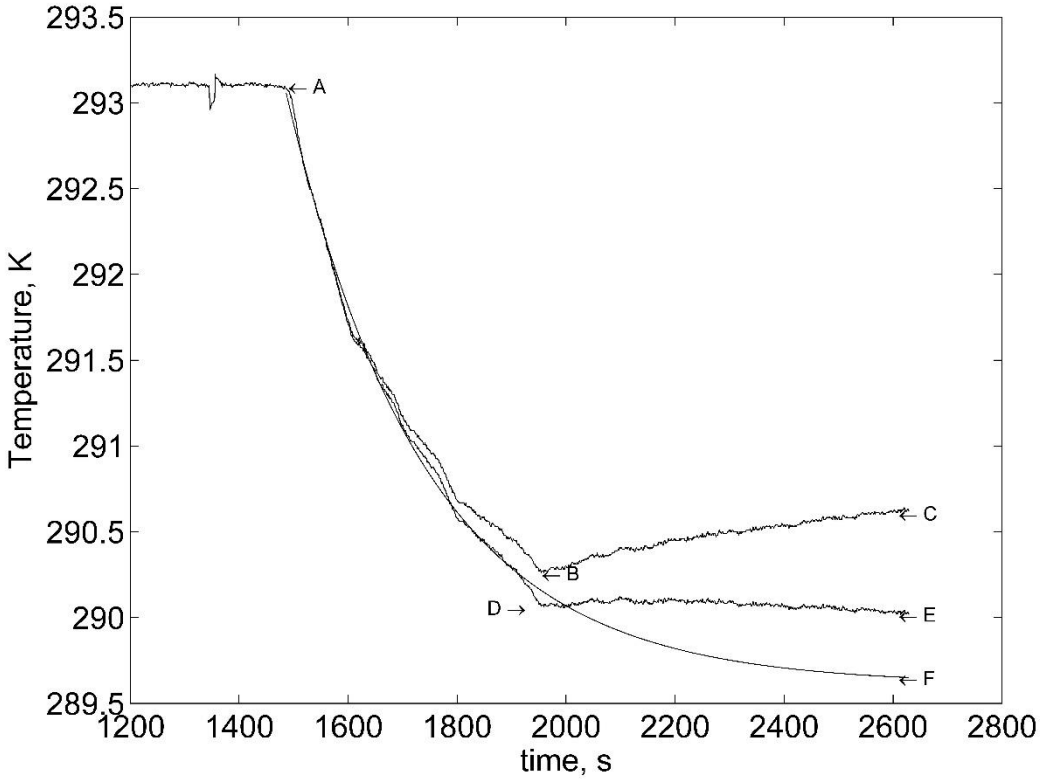

610

611 **Fig. 6 Analysis of evaporator load temperature. Point A is start of evaporation, point B is**
612 **cessation of evaporation, curve ABC is raw data, curve ADE has been corrected to estimate an**
613 **adiabatic load (using temperatures from BC), curve AF is fitted to AD and extrapolated(r^2 =**
614 **0.9972 and τ_{adiab} = 254 s)**

615

616

617

618

619

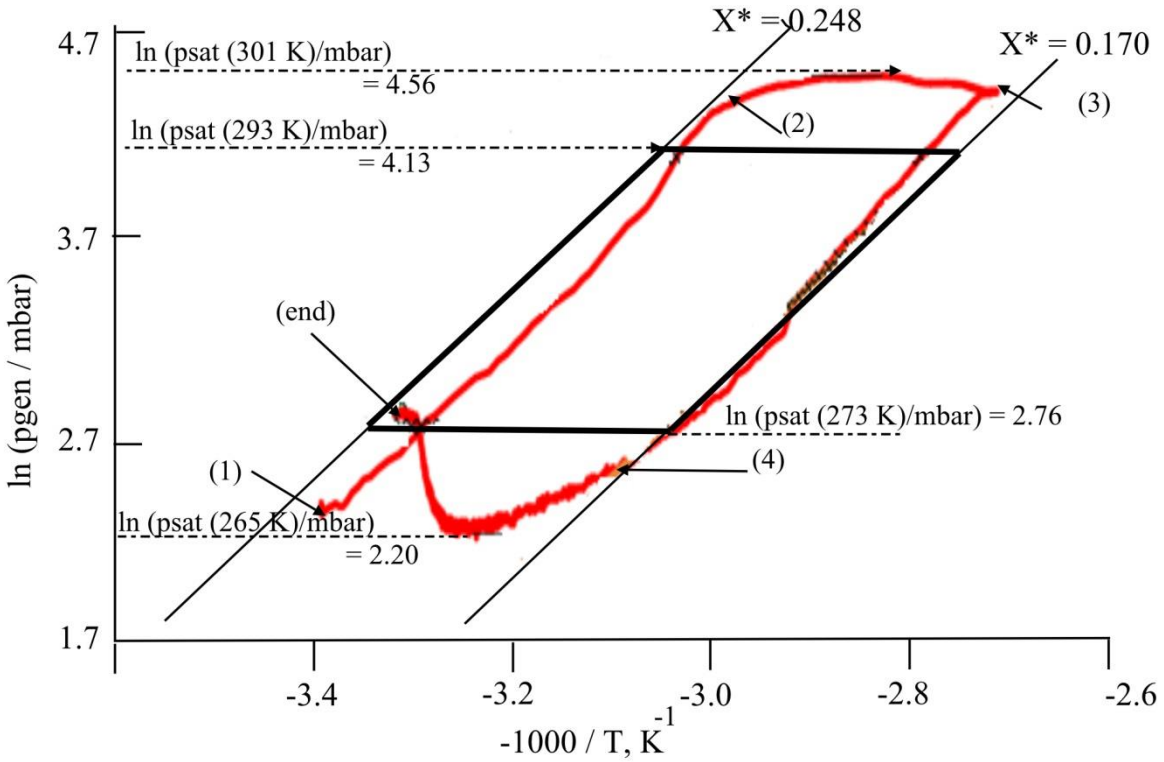

Fig. 7. Clapeyron plot of generator pressure versus ACC temperature. Cycle time = 20 minutes, the evaporator heat load is at 273 K and the condenser heat sink is at 293 K. The processes are (1)-to-(2) heating of the bed at near constant loading, (2)-to-(3) desorption of ethanol from the bed and condensation, (3)-to(4) cooling of the bed at constant loading, (4)-to-(end) adsorption of ethanol into the bed and evaporation (producing refrigeration). The bold lines show a quasi-equilibrium cycle.

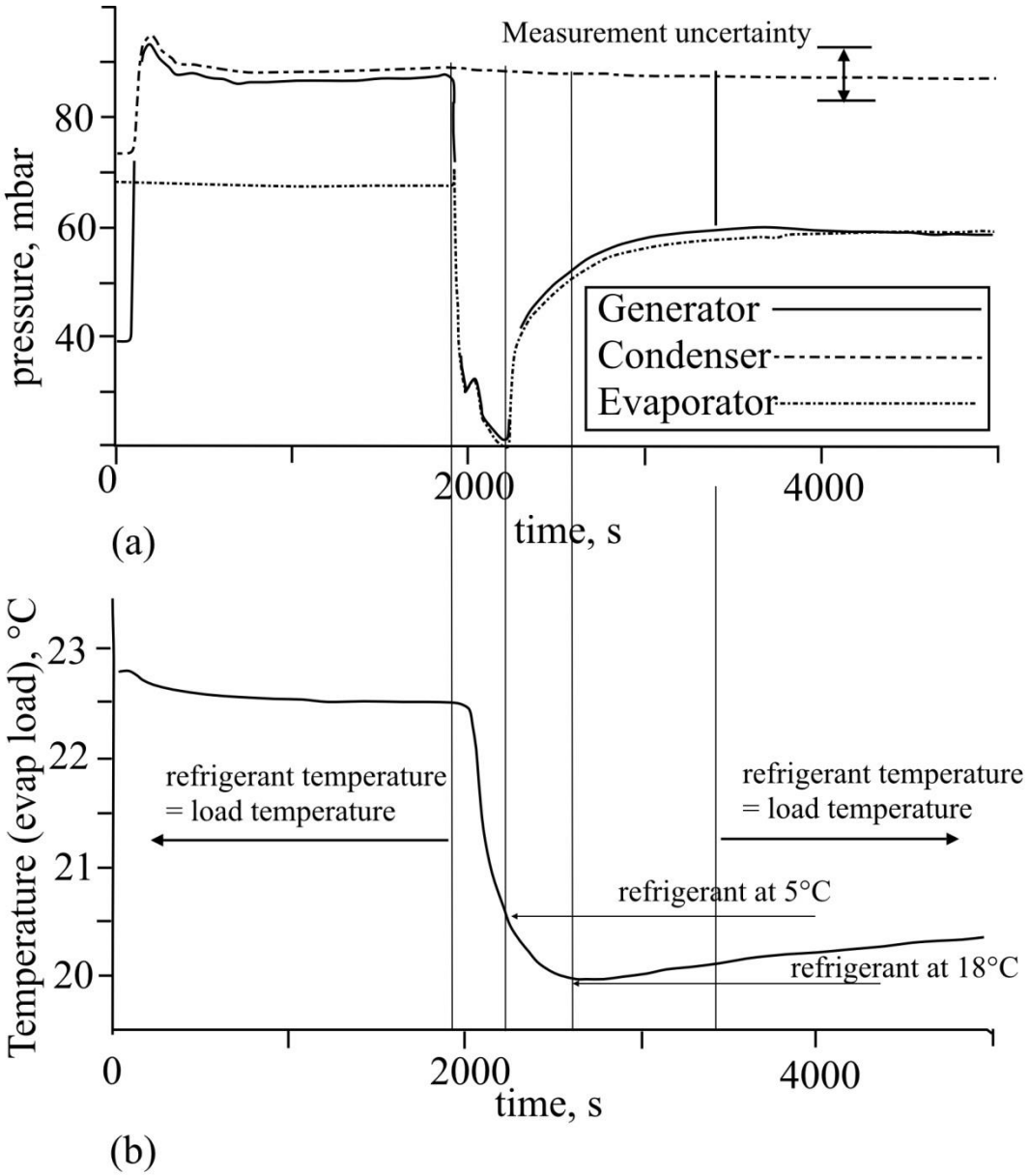

Fig. 8 Development of refrigeration pressures and impact on the evaporator load (a) pressures in the three main parts of the chiller (b) temperature of the evaporator load. The refrigerant temperatures, labelled on part (b), were calculated from evaporator pressures on part (a).

640

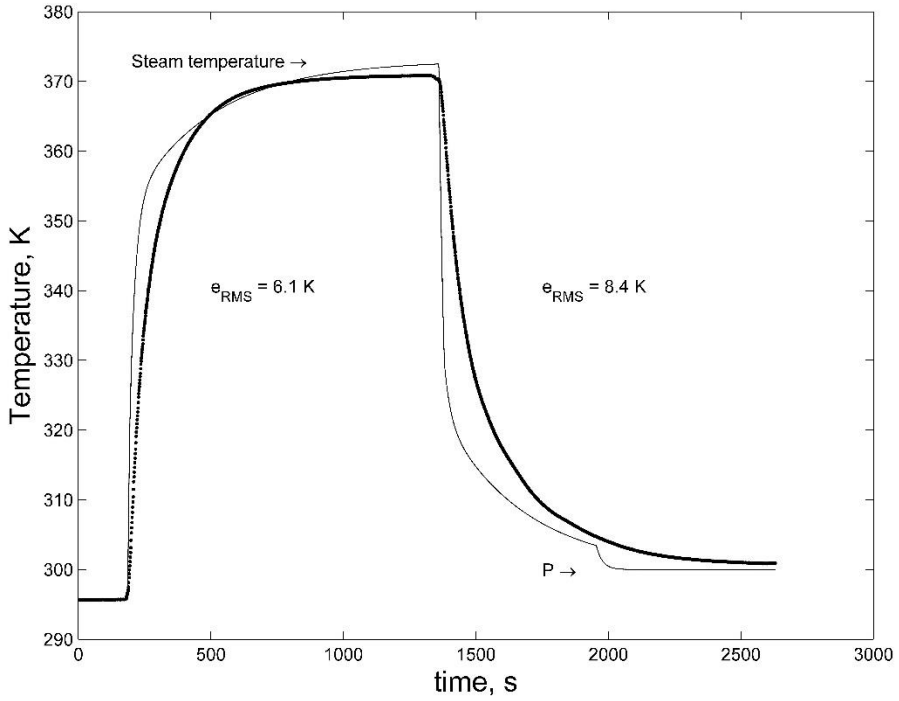

641

642 (a)

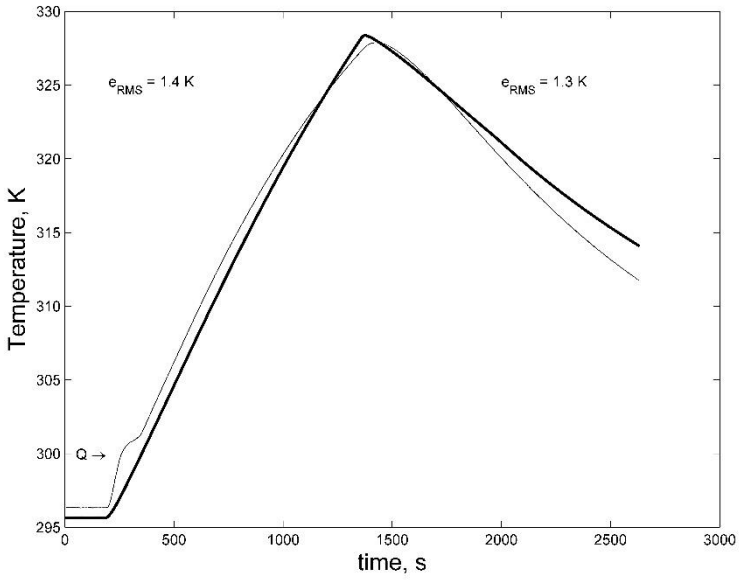

643

644 (b)

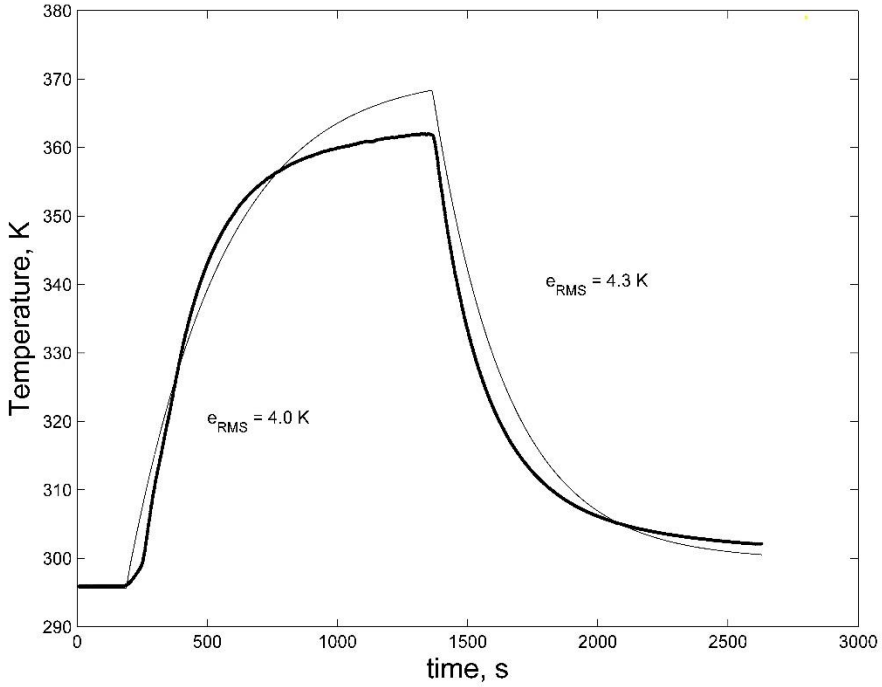

645

646 (c)

647 **Fig. 9 Selected temperatures in the generator throughout a cycle. (a) fin tip (item 17 on Fig. 1)**
648 **(b) glass cover (item 2 on Fig. 1) (c) brass plug. Thicker lines represent measured data and**
649 **thinner lines predictions.**

650

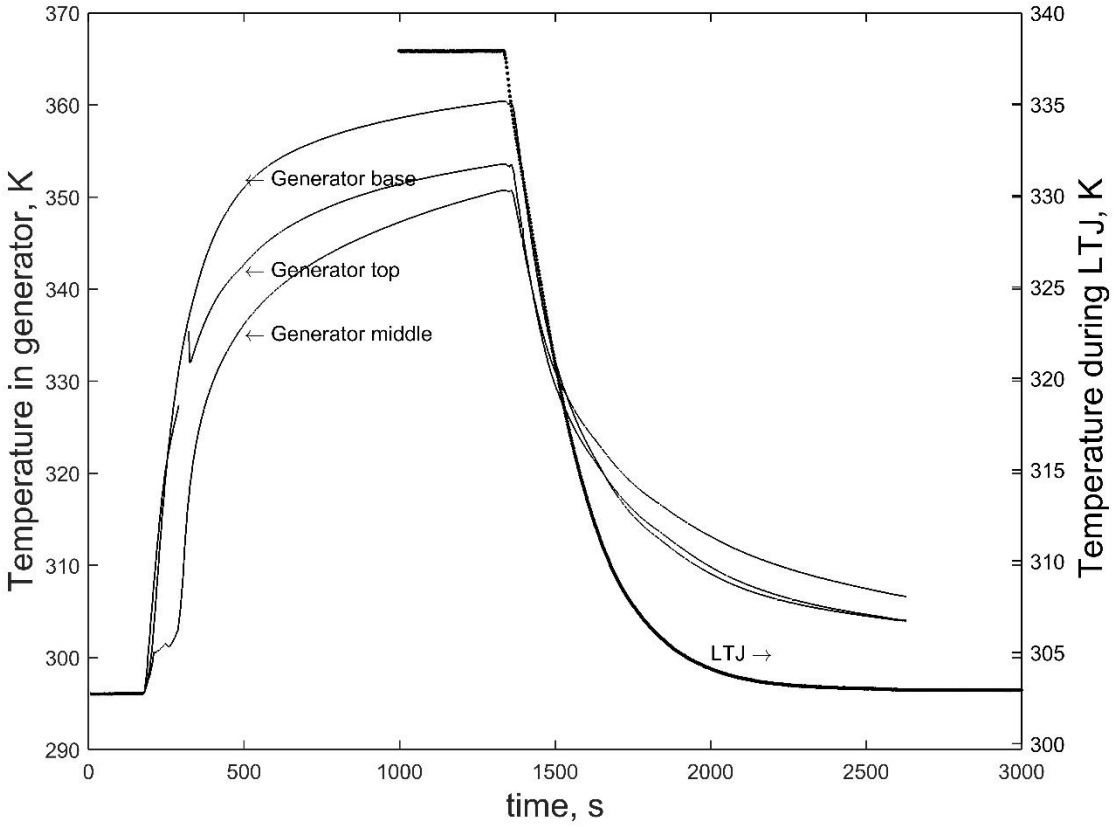

Fig. 10 Temperatures measured in the ACC mid-plane. Temperatures measured under LTJ are plotted for comparison using the right hand y-axis, starting at time = 1000 s approximately. Thermocouple positions are shown as item #18 in Fig. 1 and item #2 in Fig. 2.

Appendix A. Uncertainty Analysis

Tables 3 and 4 list expected uncertainties computed from instrument error and uncertainties in material properties. The individual uncertainties are listed in Table A1 (and reference numbers in column 1 will be referred to in this appendix). For true values X_1 and X_2, and with uncertainties $e(X_1)$ and $e(X_2)$ following a Gaussian distribution, then the uncertainty in their summation is

$$e(X_1 + X_2) = \sqrt{e(X_1)^2 + e(X_2)^2} \qquad [A.1]$$

The fractional uncertainty in their product, $e_f(X_1 X_2) = e(X_1 X_2)/(X_1 X_2)$ is

$$ef(X_1 \ X_2) = \frac{e(X_1 X_2)}{X_1 X_2} = \sqrt{ef(X_1)^2 + ef(X_2)^2} = \sqrt{\frac{e(X_1)^2}{X_1^2} + \frac{e(X_2)^2}{X_2^2}} \qquad [A.2]$$

The uncertainty analysis influences the estimate of total heat input during the heating phase, the measured COP and SCP, and the predicted COP and SCP.

A.1 The heat balance

Ten terms related to sensible heat, taking the general form

$$Q_{sens} = mc\left(T^{end} + \delta - T^{start}\right) \qquad [A.3]$$

where (in the instance of the evaporator load) δ corrects for heat ingress. The fractional error in Q_{sens} is then

$$ef\left(Q_{sens}\right) = \sqrt{ef(m)^2 + ef(c)^2 + ef\left(T^{end} - T^{start}\right)^2 + ef(\delta)^2} \qquad [A.4]$$

Scales were accurate to 0.1 g so mass errors of condenser sink (water), evaporator load, activated carbon cloth, aluminium fins, copper fins and cover glass were all better than 0.1 % and also heat capacities for these items were assumed to be well known. With regard to $e(T^{end} - T^{start})$ (1) for the condenser sink and evaporator load we took $e_2 = 0.1$ K, exceeding measured random

683 variations from a thermocouple held isothermal (2) for ACC and sorbed phase temperature $e_3 = e_5 =$
684 5 K, the standard deviation thermocouples in upper, middle and lower parts of the bed at the end of
685 heating (3) for both fins and copper, end temperatures fell 2K short of steam temperature and
686 (pessimistically) this was employed e_7 and e_8 (4) for the brass plug, predicted temperature gradients
687 were employed as uncertainty e_{10} = 5 K. The fractional uncertainty in δ was (pessimistically) taken as
688 ef_4 = 0.5. All heat capacities were taken as well known with the exception of the sorbed phase. The
689 value used was that of liquid ethanol, but [19] for example suggests a more sophisticated model
690 based on Gibbs law and Maxwell relationships. Nonetheless, in their appendix (Equation G) the
691 sorbed phase c_p will tend to liquid c_p for adsorption of an ideal gas. The deviation for measured data
692 (their Fig. 4 [19[) varies from 0% to 33% depending on loading and we take the mid-range ef_{18} = 16%
693 as an uncertainty.

694 The change of phase from sorbed to liquid contributed only 2 kJ to a total heat input of 525
695 kJ. The heat term was proportional to change in loading, $X^{end} - X^{start}$ (Equation 7 in main text)
696 estimated using adsorption capacities at equilibrium, X*. The associated fractional uncertainties
697 were ef_{16} = 13% (the standard error between the DR correlation for X^* (Equation 5) and the
698 measured data points) and from the measured time constants (final column in Table 4) the worst
699 shortfall between ΔX and ΔX^* was 29%, hence pessimistically ef_{17} = 29% giving an uncertainty in the
700 heat of phase change as $\sqrt{(0.13^2 + 0.29^2)}$ =32%.

701 Direct losses from the cover and brass plug took the form

$$Q_{direct} = A \int_{tstart}^{tend} U \, \Delta T \, dt \qquad [A.5]$$

702 and $e(\Delta T) = \sqrt{2}\, e_1$ = 1.4 K and heat losses were governed by the resistance of the polyurethane foam,
703 such that $ef(U) \approx e_{19} / \lambda_{ins}$= 0.05 /0.3 (a pessimistic uncertainty in thermal conductivity λ was taken
704 in view of the influence of temperature on λ, imperfect pipe to insulation contact and end effects).
705 Then

$$ef(Q_{direct}) \cong \sqrt{\frac{2e_1^2}{\bar{\Delta T}} + \frac{e_{19}^2}{\lambda_{ins}^2}} \qquad [A.6]$$

where a time averaged temperature difference is used on the denominator.

Uncertainties are put into Table 3; for instance in the heating/ desorption phase the uncertainties are 14%, 5%, 27% and 25% for losses from desorption processes, generator sensible heat, direct losses from the generator and sensible heat + direct losses from the pipework and Equation A.1 gives an overall uncertainty of 6% in overall heat transfer.

Heat input was determined by condensate collection: a plot of mass versus time indicated an offset of 4.8 grams, probably the condensation of steam in the trap itself, pessimisitically doubled to yield and an uncertainty of e_{15} = 22 kJ. The discrepancy between the grand total of heat terms (525 kJ) and applied heating (602 kJ) at 13% was outside the expected uncertainties and a better indicator of accuracy.

A.2 Errors in Prediction

The heat input was estimated from equations [10] or [11] in the main text. Regarding the contribution from LTJ related tests, viz

$$Q_{LTJ} = Q_{o,pred}^{(a-lx)}\left(1-\exp\left(-\frac{\tau_{1/2}}{\tau_{(a-lx)}}\right)\right) \qquad [A.7]$$

for the term $Q_{o,pred}^{(a\text{-}lx)}$ ef_{21} = 13.5% followed comparison of prediction and measurement (see Eqn 6 and Fig. 4 in main text). Putting measured $\tau_{(a\text{-}lx)}$ into the multiplier (1-exp($\tau_{1/2}/\tau_{(a\text{-}lx)}$) yielded the standard deviation and hence uncertainty ef_{23} = {0.0%, 0.1%, 0.9%} depending on $\tau_{1/2}$, the duration of half cycle. Otherwise Equations [10] and [11] hold strongly coupled terms and the procedure was not amenable to straightforward manipulation of variances, and instead the same simulation was

run 250 times with a Gaussian distribution of random errors (lines 24, 25, 26) added to each term to give an error ef_{28} = 5.4% and the total uncertainty in predicted heat input was

$$e(Q_{in}^{net,2}) = \sqrt{\left(ef_{21}^{2} + ef_{23}^{2}\right) Q_{LTJ}{}^{2} + ef_{28}^{2}\left(Q_{in}^{net,2} - Q_{LTJ}\right)^{2}}$$

For an instance where 38% of heat was attributable to QLTJ, then the fractional error of predicted heat input was ef ($Q_{in}^{net,2}$) = 5.1% and likewise the fractional error in SCP. However, it is emphasised that this account only for expected uncertainties in heat transfer coefficients and material properties, following a Gaussian pattern, and not model imperfections.

734 Table A1 **Uncertainty Analysis**

Term no	Variable	Description	Uncertainty	Explanation
	Instrument errors			
1	T	Temperatures (general)	1 K	Manufacturer's calibration claim. Systematic error.
2	T^{end} - T^{start}	Temperature changes	0.1 K	Deviations in thermocouples mounted in a constant temperature sample. Random error.
3	δ	Heat load temp. correction	0.5 δ	Half the correction applied in equation
5	Tacc	ACC temperature	5 K	Standard deviation between upper, middle and lower temperatures
6	$T_{etoh,ads}$	EtOH (sorbed)	5 K	As for ACC above
7	T_{al}	Fins (Al)	2 K	Employ closest approach to steam temperature
8	T_{HX}	HX (Copper)	2 K	As above
9	T_{cover}	Cover (glass)		Gradients from spot checks with a hand held probe.
10	T_{plug}	Plug (brass)		Gradients expected from mathematical model.
11	p	pressure	2.5 mbar	Manufacturer's claim
15	Q(steam)	Heat input	11 kJ	5 g steam required to heat collection flask to 100°C.
	Material Properties			
16	X*	Equilibrium loading	0.13 X^*	Root mean square error for DR equation reported in [11].
17	ΔX	Change in loading	0.29 ΔX	For purposes of heat balance, calculated from equilibrium values.
18	$C_{p,sorbed}$	Heat capacity sorbed phase	0.16 $c_{p,sorbed}$	
19	λ_{ins}	Insulation thermal conductivity	.05 W m^{-1} K^{-1}	(Pessimistic) estimate only, allowing for influence of temperature on lambda, imperfect pipe to insulation contact, end effects
21	$Q_o^{(a-lx)}$		0.135 $Q_o^{(a-lx)}$	Comparison with directly measured values [11] versus estimates using Equation 6
22	$\tau_{(a-lx)}$		14 s	Standard deviation from mean of 180 s, reference [11]

23	1-exp(-$\tau_{1/2}/\tau_{(a\text{-}lx)}$)		0% to 0.9% of term	
	Heat losses			
24	α_{nc}	Natural convection	0.2 α_{nc}	Churchill and Chu [ref] Fig 3., comparing data vs. fitting curve for Ra > 100.
25	α_{cond}	Condensation	0.3 α_{cond}	(Pessimistic estimate only)
26	Q_{rad}	Radiative heat transfer	0.3 Q_{rad}	Pessimistic estimate
27	$Q_{in}{}^{net,2}$ - Q_{LTJ}	Predicted heat input	0.054* ($Q_{in}{}^{net,2}$ - Q_{LTJ})	Put random errors 24, 25, 26 into prediction

735

736